Published in final edited form as:
Nature. 2015 June 25; 522(7557): 502–506. doi:10.1038/nature14559.

UbiX is a flavin prenyltransferase required for bacterial ubiquinone biosynthesis

Mark D. White[1], **Karl A.P. Payne**[1], **Karl Fisher**[1], **Stephen A. Marshall**[1], **David Parker**[2], **Nicholas J.W. Rattray**[1], **Drupad K. Trivedi**[1], **Royston Goodacre**[1], **Stephen E.J. Rigby**[1], **Nigel S. Scrutton**[1], **Sam Hay**[1], and **David Leys**[1]

[1]Centre for Synthetic Biology of Fine and Speciality Chemicals, Manchester Institute of Biotechnology, Faculty of Life Sciences, The University of Manchester, Manchester M1 7DN, UK

[2]Innovation/Biodomain Shell International Exploration and Production Inc. Westhollow Technology Center, 3333 Highway 6 South, Houston, TX 77082-3101, USA

Abstract

Ubiquinone, or coenzyme Q, is a ubiquitous lipid-soluble redox cofactor that is an essential component of electron transfer chains1. Eleven genes have been implicated in bacterial ubiquinone biosynthesis, including *ubiX* and *ubiD*, which are responsible for decarboxylation of the 3-octaprenyl-4-hydroxybenzoate precursor2. Despite structural and biochemical characterization of UbiX as an FMN-binding protein, no decarboxylase activity has been detected3–4. We report here that UbiX produces a novel flavin-derived cofactor required for the decarboxylase activity of UbiD5. UbiX acts as a flavin prenyltransferase, linking a dimethylallyl moiety to the flavin N5 and C6 atoms. This adds a fourth non-aromatic ring to the flavin isoalloxazine group. In contrast to other prenyltransferases6–7, UbiX is metal-independent and requires dimethylallyl-*mono*phosphate as substrate. Kinetic crystallography reveals that the prenyl transferase mechanism of UbiX resembles that of the terpene synthases8. The active site environment is dominated by π-systems, which assist phosphate-C1' bond breakage following FMN reduction, leading to formation of the N5-C1' bond. UbiX then acts as a chaperone for adduct reorientation, *via* transient carbocation species, leading ultimately to formation of the dimethylallyl C3'-C6 bond. The study establishes the mechanism for formation of a new flavin-derived cofactor, extending both flavin and terpenoid biochemical repertoire.

*Correspondence and requests for materials should be addressed to D.L. david.leys@manchester.ac.uk.

Author contributions

MDW carried out molecular biology, biophysical and structural biology studies together with KAPP and DL. MDW and SAM performed *in vitro* reconstitution experiments. KF and SEJR performed and analyzed EPR experiments. SH performed DFT calculations. NJWR, and DKT undertook liquid chromatography-mass spectrometry of extracts and interpreted the data on substrate-product species. All authors discussed the results and participated in writing the manuscript. DL initiated and directed this research.

Author information Coordinates and structure factors have been deposited in the Protein Data Bank under accession numbers 4ZAF, 4ZAV, 4ZAW, 4ZAX, 4ZAG, 4ZAL, 4ZAY, 4ZAN and 4 ZAZ. Reprints and permission information is available at www.nature.com/reprints.

The authors declare no competing financial interest. Readers are welcome to comment on the online version of the paper.

Europe PMC Funders Author Manuscripts

Flavin is a common cofactor responsible for highly versatile (redox)-chemistry9, its properties modified or fine-tuned by the protein scaffold, occasionally through covalent attachment to the protein matrix *via* the C6 or C8 atoms of the isoalloxazine dimethylbenzene ring10. We have shown that the reversible decarboxylases belonging to the UbiD/Fdc enzyme family require a heavily modified FMN cofactor5. In these enzymes, the FMN is linked to a C_5-alkyl group via N5-C1' and C6-C3' linkages, adding a 4th (non-aromatic) ring to the isoalloxazine ring system. Knock-out of *ubiD/fdc* or the associated *ubiX/pad* genes leads to similar phenotypes, and the latter have been shown to encode for FMN-binding proteins for which no decarboxylase activity has been detected *in vitro*2–4,11. Recently it was found that UbiX/Pad is responsible for activation of *S. cerevisiae* Fdc12, suggesting that UbiX/Pad is responsible for the synthesis of the UbiD/Fdc cofactor. The observed FMN modification by a C_5-unit suggests this occurs through prenyltransferase activity [Fig 1a].

We tested this hypothesis by incubating *Pseudomonas aeruginosa* UbiX13 with oxidized FMN and the universal isoprene precursors dimethylallyl-pyrophosphate (DMAPP) or isopentenyl-pyrophosphate (IPP). However, spectroscopic evidence for formation of a ternary isoprene precursor:FMN:UbiX complex or of covalent FMN modification could not be obtained. By contrast, perturbation in the FMN UV-visible spectrum was observed in the presence of dimethylallyl-*mono*phosphate (DMAP), leading to an apparent K_d of 12.0 ± 0.4 μM [Fig 1b]. While the minor spectral perturbation is indicative of binding close to the FMN isoalloxazine, it does not reflect FMN modification. However, reduction of the ternary FMN:DMAP:UbiX complex using sodium dithionite followed by re-oxidation under aerobic conditions leads to formation of a stable purple coloured intermediate [Fig 1c]. Ultra high performance liquid chromatography coupled with high resolution mass spectrometry of extracts from both the reduced and re-oxidized ternary FMN:DMAP:UbiX complex reveal a molecular species with mass corresponding to the reduced ($prFMN^{reduced}$) or radical ($prFMN^{radical}$) form of the UbiD/Fdc1 cofactor, respectively [Extended data Fig 1] and electron paramagnetic resonance (EPR) spectroscopy confirms the formation of a radical in ~95% yield (relative to FMN) in the reoxidized ternary complex [Fig 1d]. Furthermore, the radical species has EPR properties consistent with that of a N5, C6 alkylated flavin semiquinone [Extended data figs 2-4]. Activity of *Aspergillus niger apo*-Fdc1 could be reconstituted *in vitro* following anaerobic incubation with $prFMN^{reduced}$-UbiX. Decarboxylase activity could only be observed after exposure of the reconstituted Fdc1 to oxygen [Fig 1e], but appeared independent of the presence of UbiX [Extended data fig 5a]. No activity could be observed when incubating *apo*-Fdc1 with the $prFMN^{radical}$-UbiX. This suggests only the $prFMN^{reduced}$ form can be correctly oxidized by UbiD/Fdc1 to the corresponding reactive N5-iminium species ($prFMN^{iminium}$).

Stopped-flow experiments mixing reduced $FMNH_2$-UbiX with DMAP under anaerobic conditions reveal transient formation of a distinct spectral species [species 2 in Fig 1f] prior to formation of the $prFMN^{reduced}$ product. The rate of formation species 2 showed a hyperbolic dependence on [DMAP] with apparent K_d =730 ± 70 μM and limiting rate of k_{f1}=177 ± 7 s^{-1} [Extended data fig 5]. The decay was independent of DMAP concentration and occurred with k_{f2}=0.316±0.002 s^{-1}. Stopped-flow experiments mixing reduced

prFMN^{reduced}-UbiX with oxygen reveal that the rate of formation of the purple coloured end product is linearly dependent on oxygen concentration [Extended data fig 5].

We obtained the 1.8 Å crystal structure of *P. aeruginosa* UbiX in complex with oxidized FMN and DMAP [Fig 2a-b]. The DMAP substrate is located directly above the FMN isoalloxazine *re* face, with the dimethylallyl moiety sandwiched between the FMN and Ala89-Ser90. The dimethylallyl group is furthermore surrounded by aromatic ring systems of W84, Y169, and W200 that, together with the FMN dimethylbenzene moiety, resemble the π-cage found in other prenyltransferases or terpene synthases6–8. The phosphate moiety is bound by several cationic residues, including conserved residues R122, K129, R139 and R185 in addition to polar interactions with S90, backbone amide of Gly91, Glu140 and Tyr169 [Extended data fig. 6]. The short N5 to substrate C1' distance (3.3 Å) and relative small N10-N5-C1' angle of 98° are compatible with those observed for other flavin-substrate complexes9,14. No evidence of direct nucleophilic/oxidative attack of the oxidized FMN N5 was observed. Substrate complex crystals that are transiently reduced with sodium dithionite under aerobic conditions turned purple upon oxidation, closely resembling solution properties. The 1.6 Å crystal structure of a purple coloured crystal reveals formation of the 4-ring prFMN^{radical} [Fig 2d]. Although product formation has little effect on the active site structure, the presence of the fourth ring is accompanied by a slight rotation of the FMN at the N3 atom. This accommodates the extended isoalloxazine ring system while keeping the hydrophilic network involved in binding the isoalloxazine ring intact. These observations establish UbiX crystals are catalytically competent, but do not reveal the order in which both N5-C1' and C6-C3' linkages are made.

We used kinetic crystallography to provide detailed insights into the UbiX mechanism, taking advantage of the fact a relatively long-lived intermediate can be observed in solution studies [Fig 1f]. Reduction of the enzyme-substrate complex by sodium dithionite followed by rapid-freezing and structure determination to 1.4 Å reveals formation of an unusual N5-C1' dimethylallyl adduct occurs within 1-5 s, establishing that N5-C1' bond formation occurs first [Fig 2c]. The N5-C1' adduct adopts a significant butterfly-conformation, and the N5 is clearly sp^3 hybridized. Although Ser15 and Glu49 are located in proximity of the N5, a (transient) reorientation of both side chains is required to establish a hydrogen bonding network with the N5. The 1.9 Å structure of substrate complex crystals frozen 20-30 s following reduction reveals formation of the prFMN^{reduced} product (Extended data Fig 7). Longer incubation times lead to formation of the prFMNradical species as indicated by a gradual purple colouration of crystals. No other intermediates were seen to accumulate within the WT crystals, in agreement with our stopped-flow solution data [Fig 1f].

In order to determine whether Ser15-Glu49 are involved in N5 deprotonation and/or formation of the C6-C3' linkage, we created an E49Q variant. The mutation severely affects, but does not abolish *in vitro* Fdc1 activation (Fig 1e). While the oxidized substrate E49Q complex is similar in structure to the corresponding WT structure [Fig 3a], a distinct intermediate species was seen following reduction and rapid freezing within 1-5 seconds [Fig 3b]. While the latter structure clearly contains a reduced $FMNH_2$, no N5-C1' bond has formed, in contrast to the corresponding 1-5 s WT intermediate structure [Fig 2c]. Furthermore, both Ser15 and Gln49 establish a hydrogen bonding network with the N5. This

suggests N5 deprotonation through Ser15-Glu49 is linked to N5-C1' bond formation, a process largely rendered ineffective through the E49Q mutation [Fig 4, species $I^{reduced}$] Structures of the E49Q variant derived for crystals frozen 0.5-10 min after reduction reveal accumulation of an N5-C1' dimethylallyl adduct does occur [Fig 3c], albeit distinct in conformation from that observed in the 1-5 s WT structure [Fig 2c].

In the E49Q N5-C1' dimethylallyl adduct, the dimethylallyl substrate-derived moiety has undergone a 180° rotation when compared to the WT N5-adduct species, along with a small rotation of the isoalloxazine ring [Fig 3c; Fig 4 species IVa]. Furthermore, both Ser15 and Gln49 form a hydrogen bonding network with N5, with the Ser15-N5 hydrogen bond maintaining the N5 in an sp^3 state. This series of conformational changes achieves two objectives: a proton relay network is established between the N5 and solvent via S15 and E49, and additional space is created between the isoalloxazine dimethylbenzene moiety and Y169 to allow for formation of the 4^{th} ring.

Many of the conformational changes observed in the E49Q N5-dimethylallyl adduct are unlikely to present a significant barrier to the reaction even within the crystals. However, the observed reorientation of the dimethylallyl moiety would require substantial protein breathing motions to occur if achieved through rotation along the dimethylallyl C1-C2 bond. An alternative route through olefin isomerisation is possible, via protonation of the C2' atom (adding a *pro-S* hydrogen) with transient formation of a ternary C3' carbocation [Fig 4, species III]. The latter could reorient in the absence of active site deformation and be converted to the observed E49Q dimethylallyl–N5 adduct [Fig 4, species IVa] by abstraction of the C2' *pro-R* proton. The substrate-derived phosphate is ideally positioned to establish a proton relay network to the substrate C2', and the ternary C3' carbocation resides within a so-called π-cage made by the FMN dimethylbenzene moiety, Y169 and W200 that could assist carbocation formation. Surprisingly, despite little difference in structure, crystals of a Y169F variant are severely compromised in their catalytic ability. A similar observation is made when using $UbiX^{Y169F}$ variant for *in vitro* reconsitution of Fdc1 activity (Fig 1e). In the $UbiX^{Y169F}$ crystals, an N5-C1' DMA adduct nearly identical to that seen for the WT crystals can be readily obtained, but remains stable for several minutes [Extended data Figure 8]. This suggests Y169 is key to the conformational changes that follow formation of the first N5 adduct [Fig 4, species III], possibly through assisting proton transfer via the substrate phosphate to the dimethylallyl C2' or stabilisation of the ternary C3' carbocation.

We have been unable to trap any intermediates during formation of the dimethylallyl C3' – flavin C6 bond. We suggest C6 nucleophilic attack on the dimethylallyl C3' carbocation occurs concomitant with or following protonation of the C2' via the bound phosphate [Fig 4, species IVb]. The resulting cyclohexadiene adduct (species V) can form the final product (species VI) through aromatization concomitant with proton abstraction *via* Ser15-Glu49 [Extended data Fig 9]. We suggest the E49Q mutation also affects this particular deprotonation, leading to the accumulation of an intermediate (species IVa) preceding this step as observed in the crystals. It is possible that formation of the cyclohexadiene adduct (V) occurs directly following conformational change of the C3' carbocation species (III), via species IVb without intermediate deprotonation/protonation as outlined for species IVa.

In addition to UbiX, a distinct family of flavoenzymes (type 2 isopentenyl diphosphate isomerases) bind isoprene precursors. The latter have been suggested to use the flavin as an acid-base in the interconversion of IPP and DMAPP15–16. Instead, our data reveal UbiX has many similarities to terpene synthases, achieving the required isoprenyl chemistry via similar strategies [Fig 4] 8,17–18. We suggest formation of an initial allylic carbocation through leaving of the phosphate group (pyrophosphate in the terpene synthases) is achieved through stabilization of the carbocation species within an active site dominated by π-systems (i.e. the π-cage). Furthermore, FMN reduction appears to act as the trigger for phosphate-C1' bond breakage, increasing the electron density of the isoalloxazine ring that stacks with the dimethylallyl substrate. In contrast to the metal requiring terpene synthases, the leaving group is stabilized by a multitude of ionic interactions. A direct contact with the conserved Glu140 furthermore suggests phosphate protonation occurs concomitant with C1' allylic carbocation formation and/or N5 nucleophilic attack [Fig 4, species $I^{reduced}$). Following formation of the N5-C1' bond, UbiX appears to act as a chaperone for substrate reorientation (conversion of species III to IVb), similar to what is postulated to occur for terpene synthases. In UbiX, it appears both the leaving group phosphate as well as a conserved Tyr residue (Y169) are involved in catalysing the conformational change of the N5 adduct required for completion of the reaction.

The presence of *ubiX/ubiD*-like genes in the majority of microbes2,19–21 and the essential role played in prokaryotic ubiquinone biosynthesis2 suggest an ancient evolutionary origin for the UbiX flavin prenyltransferase chemistry. It remains unclear at this stage why dimethylallyl-*mono*phosphate is used by UbiX, as opposed to the universal dimethylallyl-diphosphate22. This might serve as a means to regulate product formation via availability of DMAP. While the isomer isopentenyl monophosphate has recently been shown to occur in certain archaea23, the metabolic route to dimethylallyl-monophosphate remains unclear. The unusual biochemical strategy of using a reduced - rather than oxidized- flavin to act as a nucleophile9,24–25 ensures formation of a relatively stable N5-alkyl adduct species ($prFMN^{reduced}$), as opposed to the corresponding N5-iminium adduct ($prFMN^{iminium}$). The latter would be prone to hydrolysis prior to transfer to *apo*-UbiD/Fdc1. Whether non-*ubiD* related enzymes make use of the novel chemical properties of the UbiX product remains to be established.

Material and methods

Cloning of *P. aeruginosa* UbiX for heterologous expression in *E. coli*

The *ubix* gene of *Pseudomonas aeruginosa* was amplified from synthesized DNA (codon optimized for expression in *Escherichia coli*, Genescript) by PCR using Phusion polymerase (NEB). The PCR products were cloned in to the NcoI and HindIII restriction sites of the pNIC28a-Bsa4 vector using ligation independent methods (Infusion HD, Clontech). This generated a construct with an N terminal polyhistidine tag and TEV protease cleavage site similar to that used in ref 12. The Infusion product was transformed into *E.coli* NEB5α competent cells (NEB) to allow verification of the expression construct by sequencing (Eurofins). Validated pNIC28-Bsa4-*ubix* was transformed into *E.coli* BL21 (DE3) competent cells (NEB) for protein production.

Cloning of *A.niger* Fdc1 for heterologous expression in *E.coli*

The *A. niger fdc*1 gene was codon optimized to remove codons that were rare in *E. coli* and synthesized (Genscript) in pUC57. The gene was excised out of pUC57 using *Nde*I and *Xho*I, cloned into the *Nde*I and *Xho*I sites of pET30a using T4 ligase (NEB) and transformed into *E. coli* NEB5α. Once the sequence of the insert was confirmed *A. niger* Fdc1 pET30a was transformed into *E. coli* Bl21(DE3).

Mutagenesis of *P. aeruginosa* UbiX for heterologous expression in *E. coli*

Mutagenesis primers were designed using the QuikChange Primer Design Program (www.genomics.agilent.com/primerDesignProgram.jsp) to be used in conjunction with Phusion polymerase mediated PCR. Template DNA was removed by DpnI (NEB) digest and the PCR products were transformed into *E. coli* NEB5α competent cells to allow mutagenesis to be verified by sequencing. Constructs possessing validated mutations were transformed into *E. coli* BL21 (DE3) competent cells for protein production.

Heterologous expression of *P. aeruginosa* UbiX (WT and variants) and *A. niger* Fdc1

E. coli transformants were grown in 1l of Luria-Bertani (LB) broth at 37°C/180rpm until an OD_{600} of 0.6 – 0.8 was reached. Cultures were induced with 0.3mM IPTG and grown overnight at 20°C/180rpm. Cells were harvested by centrifugation at 7000g for 10 minutes.

Purification of *P. aeruginosa* UbiX WT and variants

Cell pellets were re-suspended in 50mM Tris, 500mM NaCl pH 8.0 buffer supplemented with lysozyme, RNase, DNase (Sigma) and a Complete EDTA free protease inhibitor cocktail (Roche). The cells were lysed using a French Press cell disrupter at 1500 Psi followed by centrifugation at 48000g for 30 minutes and filtration through a 0.45 micron membrane. The soluble supernatant was loaded on to equilibrated Ni-NTA agarose resin (Qiagen) and washed successively with 4 column volumes of re-suspension buffer containing 10 and 40mM imidazole. The protein was eluted with 250mM imidazole and analysed by SDS-PAGE to verify sample purity. Imidazole was removed using a 10-DG desalting column (Bio-rad) equilibrated with 20mM Tris, 200mM NaCl pH 8.0. Where necessary the samples were incubated with 10mM FMN to improve flavin occupancy in the protein. Excess FMN was removed before experimentation by desalting, as described above. The N terminal polyhistdine tag was retained for all experiments.

Purification of *A. niger* Fdc1

A. niger Fdc1 was purified as described above using 50mM Tris, 200mM NaCl pH 7.5 as the re-suspension buffer and 20mM Tris, 100mM NaCl pH 7.5 as the desalting buffer.

UV-visible spectrometry and protein quantification

UV-visible absorbance spectra were recorded using a Cary UV-visible spectrophotometer. Protein concentrations were estimated from A_{280} using their respective absorbance coefficients, which were calculated from their primary amino acid sequence using the ProtParam program on the ExPASy proteomics server. Wild type and E49Q *P. aeruginosa* UbiX ε_{280} = 16960M^{-1} cm^{-1}, Y169F ε_{280} =15470 M^{-1} cm^{-1} and W200F ε_{280} = 11460M^{-1}

cm^{-1}. The concentration of *A.niger* Fdc1 and FMN were estimated using ε_{280} = 68870M^{-1} cm^{-1} and ε_{450} = 12500M^{-1} cm^{-1} respectively.

Analysis of DMAP binding to *P. aeruginosa* UbiX

Distinct perturbations in the absorbance profile of FMN allowed the binding of DMAP to be monitored using UV-visible spectroscopy. The effects of titrating minimal volumes of 12.5μM DMAP on the absorbance spectrum of 30μM UbiX:FMN were recorded and converted to difference spectra by subtracting titrated profiles from the DMAP-free sample. The dissociation constant of DMAP was determined by analyzing the total deviation in absorbance between 310 and 540nm in function of DMAP concentration using the tight binding equation

Reduction and oxidation of *P. aeruginosa* UbiX WT and variants for UV-visible spectroscopy and EPR analysis

All anaerobic work was performed under N_2 in a glove box (Belle Technology, UK). 150μM *P. aeruginosa* UbiX:FMN was rendered anaerobic in 20mM Tris, 200mM NaCl pH 8.0 and mixed with 1mM DMAP to monitor the effect of redox cycling on flavin properties. Sodium dithionite was titrated into the sample to fully reduce the FMN, which was subsequently re-oxidized. UV-visible spectra were recorded at each stage and 300μl aliquots were isolated for EPR analysis.

Preparation of cofactor extracts for mass identification

The oxidized product of UbiX turnover was extracted from *P. aeruginosa* UbiX under aerobic conditions by denaturing the protein with equal volumes of acetonitrile at 70°C. Precipitate was removed by centrifugation at 16000g for 10 minutes. The resulting supernatant was sent for high-resolution mass analysis.

The reduced product of UbiX turnover was generated under anaerobic conditions from a steady state reaction containing 1mM $FMNH_2$, 1mM DMAP and 20μM *P. aeruginosa* UbiX. Protein was removed by precipitation at room temperature as described above. The resulting supernatant was sent for analysis by high-resolution mass spectrometry.

Stopped-flow kinetics of *P. aeruginosa* UbiX

The kinetics of a single turnover reaction between UbiX:$FMNH_2$ and DMAP was studied under anaerobic conditions on a SX.18MV-R stopped-flow spectrophotometer (Applied Photophysics, dead time approximately 1 ms) by measuring changes in the flavin absorbance spectrum logarithmically over 60 seconds using a photodiode array (PDA) detector. 100μM UbiX:FMN was rendered anaerobic in 20mM Tris, 200mM NaCl pH 8.0 and supplemented with 1mM glucose, 10U ml^{-1} glucose oxidase (Sigma) to guarantee an oxygen free environment. The protein was reduced with sodium dithionite before being rapidly mixed with equal volumes of 500μM – 4mM DMAP at room temperature. The spectral intermediates were resolved by singular value decomposition using the Pro-Kineticist program (Applied Photophysics). Data could be fitted with minimum residuals to a three step model (A>B>C>D), which allowed the rate constants k_{f1}, k_{f2} and k_{f3} to be

Europe PMC Funders Author Manuscripts

estimated. Species D was identified as a photoinduced adduct and considered an artifact of the prolonged illumination required.

The kinetic parameters of a single turnover reaction between UbiX:prFMN^{reduced} and oxygenated buffer were measured using a stopped flow instrument (see above). Here 100μM UbiX:FMN was rendered anaerobic (in the absence of glucose oxidase), before being reduced with dithionite and mixed with 1mM DMAP. The protein was rapidly mixed with equal volumes of 0 – 100% oxygenated buffer, producing absorbance spectra that could be analyzed by single value decomposition. Data were fitted to a one step model (A>B), which allowed the rate constant k_{AB} to be estimated.

In vitro reconstitution of *A. niger* Fdc1

For reconstitution under steady state conditions, a solution containing 1mM $FMNH_2$, 1mM DMAP and respectively wild type *P. aeruginosa* UbiX, E49Q or Y169F was incubated with 50μM apo-*A. niger* Fdc1 in 20mM Tris, 200mM NaCl, 1mM $MnCl_2$ pH 8.0 under anaerobic conditions. The specific activity of reconstitued Fdc1 with 50μM cinnamic acid (in 50mM KPO_4, 50mM KCl pH 6.0; either aerobic or anaerobic) was determined at regular time intervals by measuring the rate of decarboxylation at 270nm using a Cary UV-visible spectrophotometer.

Reconstitution experiments using a filtered UbiX reaction were carried out using 2mM $FMNH_2$ anaerobically incubated overnight with 5mM DMAP and 50μM UbiX. This reaction mixture was used to reconstitute *A. niger apo*-Fdc1 (supplemented with Mn^{2+}) in a 2:1 molar ratio, assuming complete conversion of $FMNH_2$ to prFMN^{reduced}. To obtain filtrate devoid of UbiX, the reaction mixture was anaerobically filtered in 10K MWCO centrifugal concentrator (Generon). A negative control with DMAP omitted from the overnight reaction was also performed. Decarboxylase activity was measured using as 800μM aerobic cinnamic acid.

Crystallization of *P. aeruginosa* UbiX WT and variants

7.5mg/ml *P. aeruginosa* UbiX in 20mM Tris, 200mM NaCl pH 8.0 was supplemented with 0.5mM FMN and mixed with 1mM DMAP to promote ligand binding in the active site. Initial screening, sitting 0.3μl protein and 0.3μl mother liquor next to 50μl reservoir, yielded a variety of hits after 1 – 2 days at 25°C. The best crystals were obtained after 1 – 2 days in 12% PEG 3350, 150mM sodium thiocyanate, and 100mM Tris pH 7.2 at 25°C. Crystals of the UbiX variants were obtained in the same conditions.

Diffraction data collection and structure elucidation

All crystals were cryoprotected in mother liquor supplemented with 10% PEG 200 and flash cooled in liquid nitrogen. Reaction intermediates were obtained by flash cooling crystals that had been incubated in cryoprotectant containing sodium dithionite. Where periods of long soaking were necessary, the cryoprotectant was also supplemented with FMN and DMAP to reduce dissociation from the crystals. Diffraction data was collected up to 1.4Å at Diamond beamlines at 100K and processed using the CCP4 suite25. Data was reduced and scaled using XDS26. The structure of *P. aeruginosa* UbiX was refined using REFMAC5, using

3ZQU as te starting model, and refined by cycles of manual rebuilding in COOT and additional processing in REFMAC525. Ligand coordinates and definitions were generated using the GlycoBioChem PRODRG2 server (http://davapc1.bioch.dundee.ac.uk/cgi-bin/prodrg). The data and refinement statistics are available in Extended Data Table 1.

Mass spectrometry

All solvents were of HPLC-MS grade and purchased from Sigma–Aldrich (Gillingham, UK). HPLC grade formic acid was purchased from Fisher Scientific (Loughborough, UK). Mass spectrometer calibration solution and chromatography columns were purchased from Thermo-Fisher Scientific (Hemel Hempstead, UK).

All UHPLC-MS work was carried out on a Thermo-Finnigan Orbitrap-LTQ XL™ hybrid mass spectrometer operated in negative ionization mode coupled to a Thermo Accela autosampler (Fisher Scientific, Bremen, Germany). Chromatographic separations were adapted from work carried out by Fu and co-workers27 and performed on a Thermo Hypersil Gold 2.1μm C_{18} column at a solvent flow-rate of 400 μL min^{-1}. For initial profiling tests the column was eluted with 0.1% formic acid in water (A) and 0.1% formic acid in acetonitrile (B). The solvent composition during gradient elution was initiated with 5% (B) for 5 min and subsequently ramped to 95% (B) over 15 min, followed by a 5 min isocratic elution at 95% (B) before a return to 95% (A) held for further 5 min for column equilibration. All samples were maintained at 4 °C within the autosampler refrigerator whilst the column was maintained at 50°C within the autosampler oven. Mass calibration was carried out in accordance with the manufacturer's guidelines using caffeine, the tetrapeptide MRFA and Ultramark 1621 in an acetonitrile/methanol/acetic acid solution. Acquisition settings for initial profiling were carried out at 60,000 resolution in centroid and ran at 1 μ-scan per 400ms in the 100-1000 *m/z* range with source gasses set at Sheath Gas = 40 arb units, Aux Gas =5 arb units, Sweep Gas = 5 (all systems specific arbitrary units). The ESI source voltage was set to 4.2V, and capillary ion transfer tube temperature set at 275°C.

Mass fragmentation analysis was carried out with the same column chemistry, source settings and flow rate but with an isocratic solvent elution of 55% (A) / 45% (B), an optimum composition determined for eluting the analyte of interest, based on the initial elution profile described above. MS source, sample storage/column was kept under identical conditions. Collision Induced Dissociation (CID) settings were set up to trap target ions with an isolation width of 1.0 *m/z*, normalized collision energy of 35, activation Q of 0.250 and activation time of 30 ms.

EPR spectroscopy

Continuous wave X-band (~9.4 GHz) EPR spectra were obtained using a Bruker ELEXSYS E500 EPR spectrometer operating at cryogenic temperatures via an Oxford Instruments ESR900 liquid helium cryostat interfaced with an ITC503 temperature controller from the same manufacturer. Samples were 250 μl in Wilmad 4 mm o.d. quartz tubes. Sample temperatures were as stated, microwave power was 10 μW, modulation amplitude was 1.5 G. Pulsed electron nuclear double resonance (ENDOR) spectra were obtained at 65 K using a Bruker ELEXSYS E580 spectrometer equipped with an EN 4118X-MD4 dielectric

resonator. Temperature control was effected using an Oxford Instruments CF935 cryostat and ITC503 temperature controller. The Davies pulsed ENDOR sequence was employed at intermediate Q using soft microwave pulses and FID detection ($\pi/2$ = 200 ns) with a 9 ms radiofrequency π pulse.

DFT calculations

Density function theory (DFT) models of FMN:DMA adducts were optimised in the gas phase using the (U)BP3LYP/6-311++G(d,p) level of theory implemented in Gaussian 09 [28]. The models consist of an FMN truncated after the 2' carbon and 2-methyl-2-butene, i.e. the dephosphorylated DMAP (Extended data Fig. 4). Structural alignments to the crystal coordinates were performed using Swiss-PdbViewer version 4.1 [29]. Harmonic vibrational frequencies calculated using normal mode analysis were used to confirm that optimised geometries were always in local or global minima.

Europe PMC Funders Author Manuscripts

Extended Data

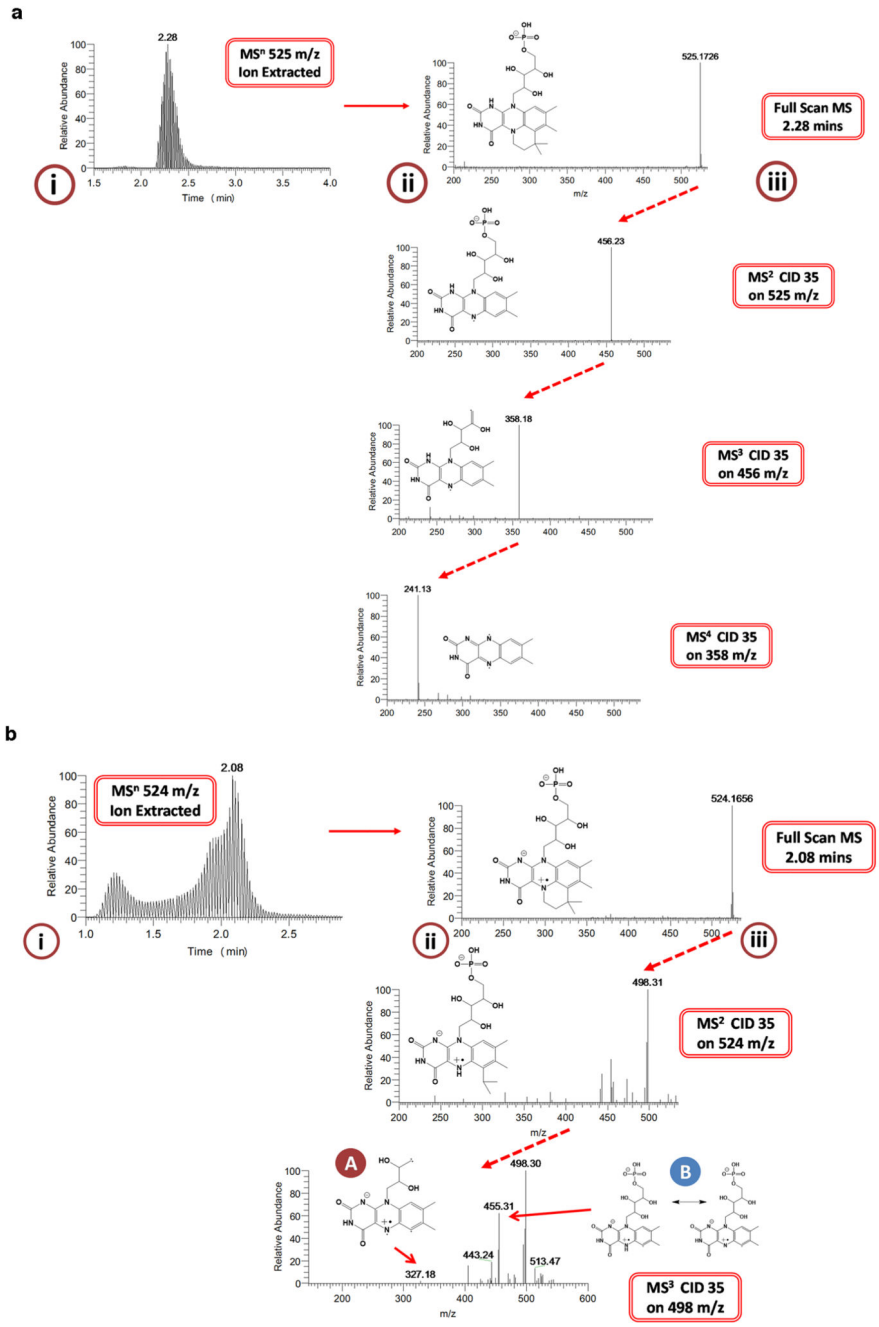

Extended Data Figure 1.

a: Structural elucidation of the reduced UbiX/Fdc1 co-factor. From an initial full scan TIC on UbiX/Fdc1 extract, a 525 *m/z* ion extracted chromatogram was created under a gradient elution using H_2O/ acetonitrile both containing 0.1% Formic Acid indicating a major peak apex at 9.57 mins with a 54/46 solvent elution composition (not shown). Subsequent data dependant TIC and 525 *m/z* scan extracted chromatograms were created under 55% A / 45%

Europe PMC Funders Author Manuscripts

B isocratic solvent elution and ion extraction between 524.5-525.5 *m/z* produced a singular peak at 2.28mins displaying an associated full scan molecular ion peak with *m/z* = 525.1726 ($M^+ = C_{22}H_{30}N_4O_9P$) at a resolution of 58,500 with a mass accuracy of 3.59 ppm. Fragmentation of the 525.1726 *m/z* molecular ion peak in an automated data dependent manner using helium based-chemical induced dissociation (CID level 35) generated a spectral tree that indicates the removal of the newly formed, more labile, tertiary ring at the MS^2 level. Subsequent removal of the phosphate head group at the MS^3 level was achieved using CID 35 on the 456.23 *m/z* molecular species with a final MS^4 step using CID 35 on 358.18 *m/z* completely removing the tail group from the central 3-ring isoalloxazine system. **b:** Structural elucidation of the re-oxidised UbiX/Fdc1 co-factor. From an initial full scan TIC on UbiX/Fdc1 extract **(i)**, a 524 *m/z* ion extracted chromatogram was created under a gradient elution using H_2O/ acetonitrile both containing 0.1% Formic Acid indicating a major peak apex at 9.24 mins with a 48/52 solvent composition (not shown). Subsequent data dependant TIC and 524 *m/z* scan extracted chromatograms **(ii)** were created under 50% A / 50% B isocratic solvent elution and ion extraction between 523.5-524.5 *m/z* produced a singular peak at 2.08mins displaying an associated full scan molecular ion peak with *m/z* = 524.1656 ($M^+ = C_{22}H_{29}N_4O_9P$) at a resolution of 58,500 with a mass accuracy of 2.78 ppm. Fragmentation of the 524.1656 *m/z* molecular ion peak in an automated data dependent manner using helium based-chemical induced dissociation (CID level 35) generated a spectral tree **(iii)** that indicates the removal of the newly formed, more labile, tertiary ring at the MS^2 level. Subsequent removal of the phosphate head group at the MS^3 level was achieved using CID 35 on the 498.31 *m/z* molecular species to create 327.18 (A) alongside a sister fragment 455.31 (B) that represents the full removal of the tertiary ring but retaining the phosphate head group.

Europe PMC Funders Author Manuscripts

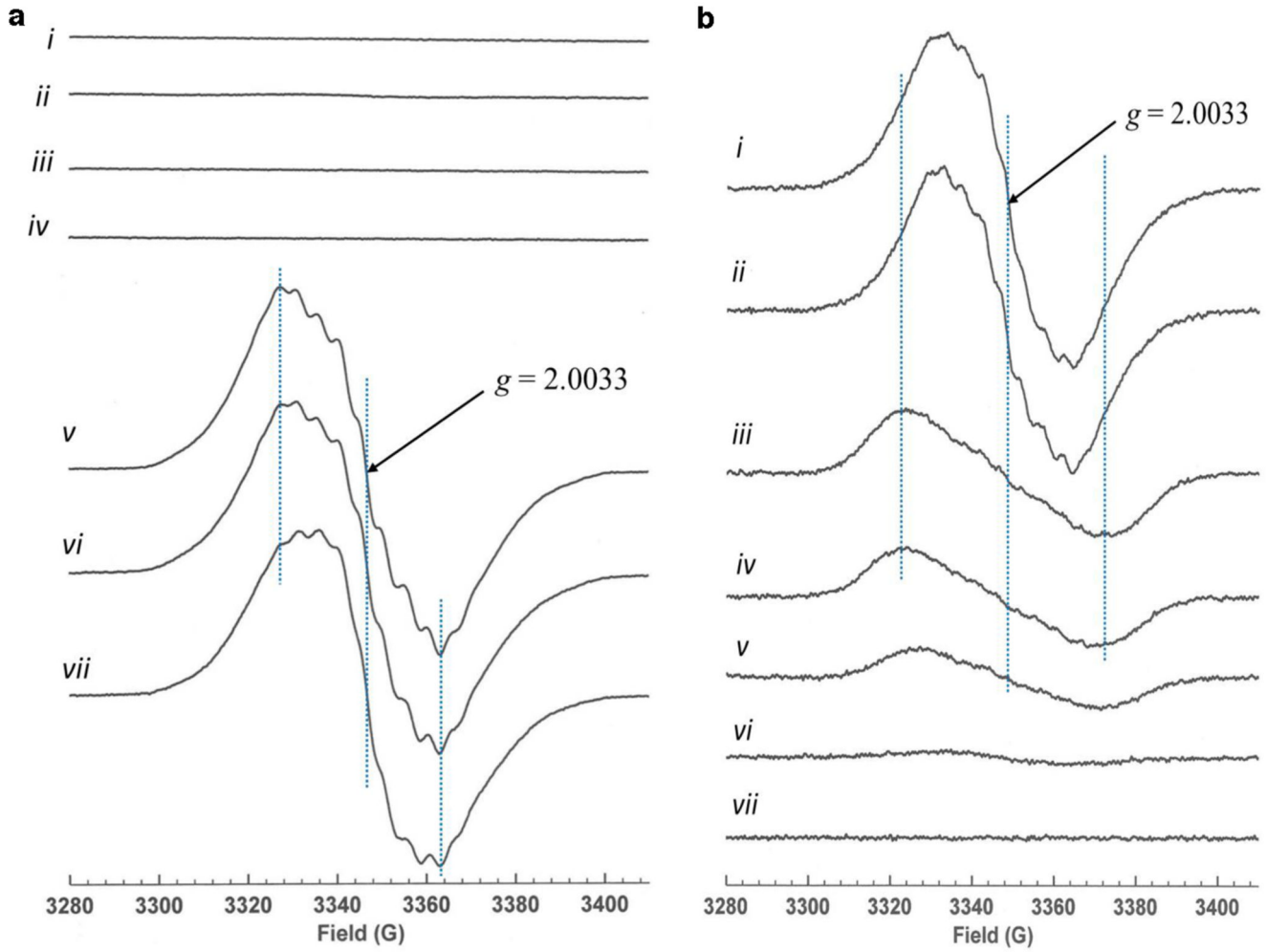

Extended data Figure 2.

Panel A. X-band continuous wave EPR spectra of UbiX in frozen solution: i) WT as isolated; ii) WT plus DMAP; iii) WT reduced with dithionite; iv) WT + DMAP reduced with dithionite; v) WT + DMAP reduced with dithionite and reoxidised with oxygen; vi) Y169F mutant + DMAP reduced with dithionite and reoxidised with oxygen; vii) W200F mutant + DMAP reduced with dithionite and reoxidised with oxygen. Clearly the FMN-DMAP adduct radical is only formed when UbiX is reoxidised in the presence of DMAP and this formation is not affected by mutation of those aromatic residues forming the π-cage that could give rise to Y or W radical species. Panel B. X-band continuous wave EPR spectra of frozen solutions of WT UbiX + DMAP and reduced with dithionite with the addition of potassium ferricyanide to the following concentrations: i) 260 μM; ii) 160 μM; iii) 50 μM; iv) 40 μM; v) 30 μM; vi) 20 μM; vii) 0 μM. Experimental conditions: microwave power 10 μW, modulation amplitude 1.5 G, temperature 20 K. Showing the radical can also be formed using chemical oxidation in the absence of oxygen and thus does not arise from a peroxide species generated by the reaction of reduced oxygen species formed when the dithionite sample is exposed to oxygen. An initial radical is formed under these conditions

that exhibits a considerably broader EPR signal than the prFMN^{radical} and is as yet unidentified.

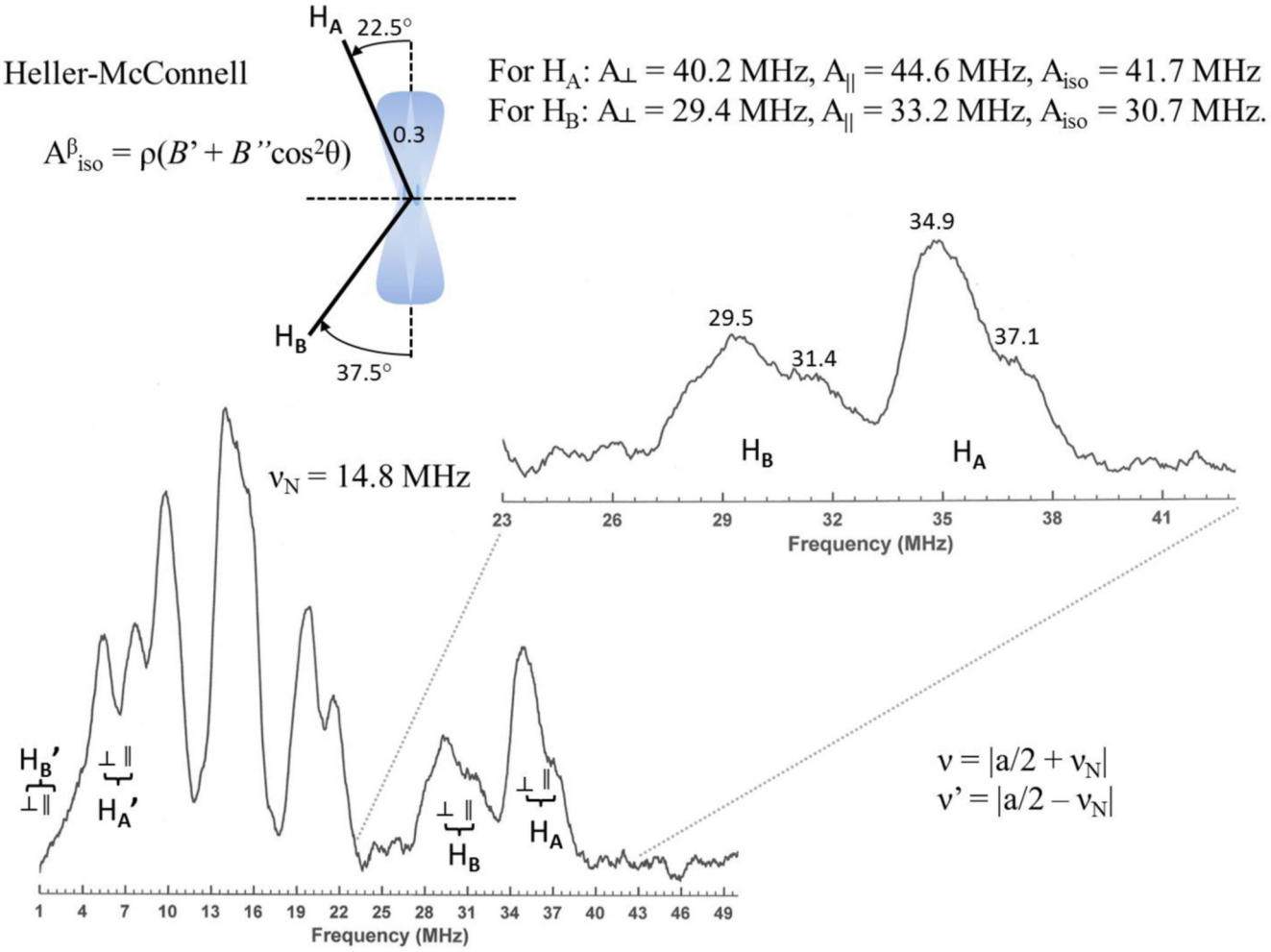

Extended Data Figure 3.

Pulsed Davies ENDOR spectra of the prFMN^{radical}:UbiX complex. The spectrum was measured at a field equivalent to g_{av} = 2.0033. While a complete assignment of the spectrum requires specific deuteration of FMN and DMAP, the ENDOR spectrum is dominated by two large hyperfine couplings to β-protons indicated as H_A and H_B. Using the Heller-McConnell equation the values of the dihedral angles, θ, can be determined as shown and are consistent with the orientation of the C1'-protons of the DMAP-derived fragment of the radical observed crystallographically, as shown in the figure above. The unpaired electron spin density, ρ, at N5 of the FMN-derived fragment of the radical can also be estimated from the Heller-McConnell equation. B' is negligible while B" is thought to have a value of ~160, although studies of β-protons coupled to unpaired electron spin density at a nitrogen atom are rare, giving an unpaired spin density at N5 of ~0.3, consistent with calculations and considerably smaller than the unpaired electron spin density of 0.4 or greater expected for C1' of an aromatic amino acid radical.

Europe PMC Funders Author Manuscripts

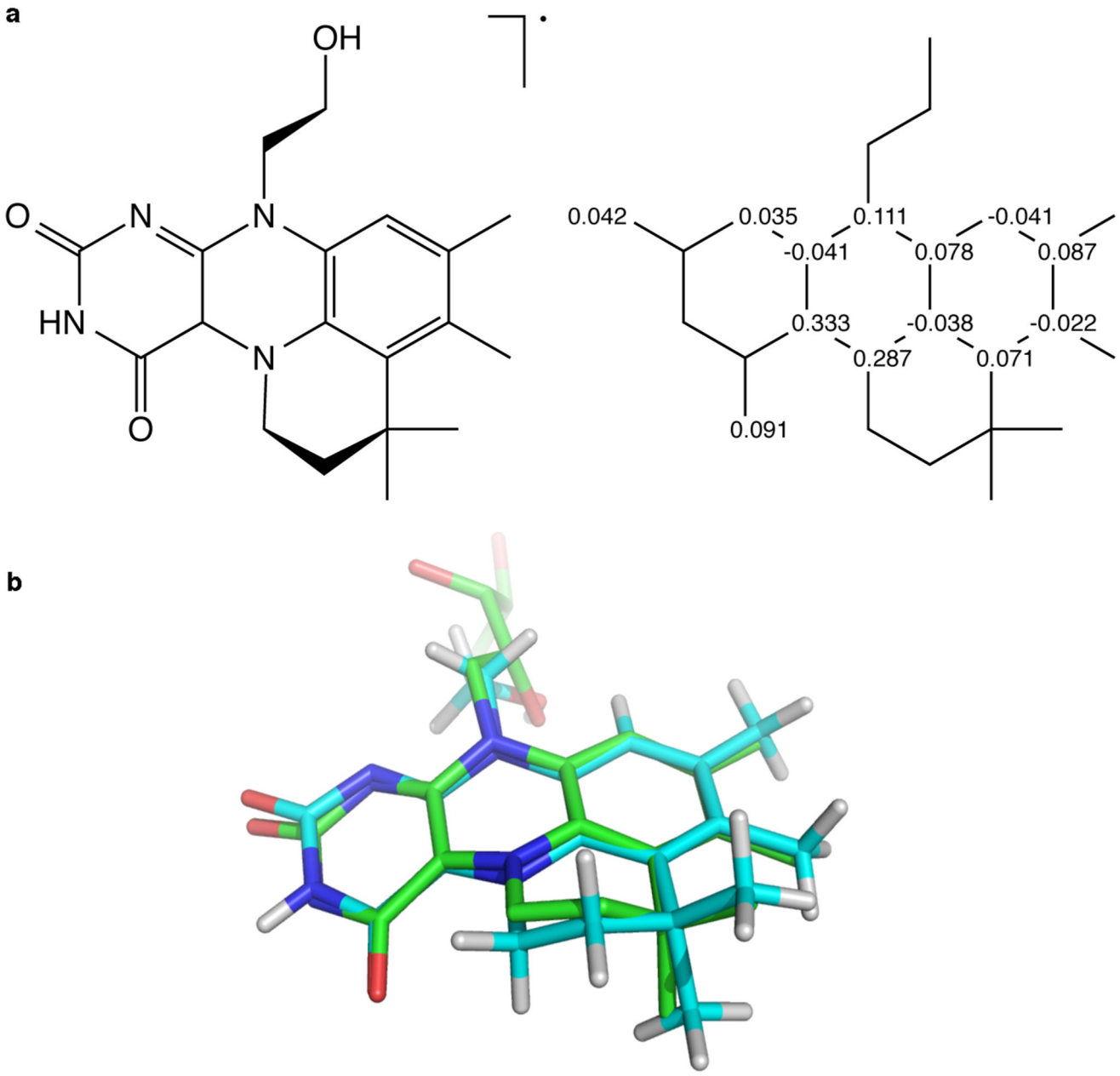

Extended Data Figure 4.

Top, DFT model of the purple radical species showing the location of significant atomic spin densities (>|0.02|) to the right. The optimised structure (blue carbons) overlaid with the crystal coordinates (green carbons) is shown below. The model was geometry optimised in the gas phase using the UB3LYP/6-311++G(d,p) level of theory. Cartesian coordinates of the optimised structure are given in Supplementary Information.

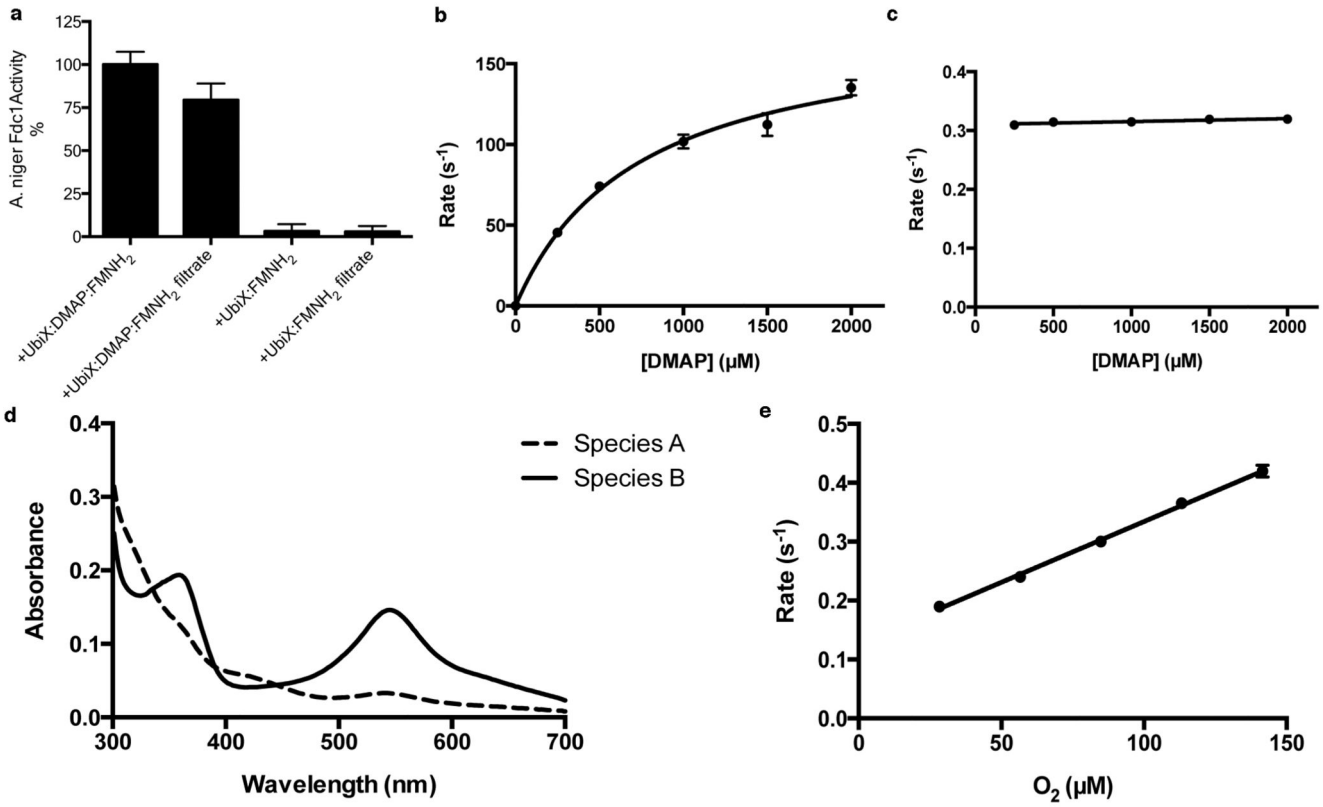

Extended Data Figure 5.

A) Reconstitution of *A. niger* Fdc activity with UbiX:prFMN^{reduced} and prFMN^{reduced} obtained through filtration of a UbiX:prFMN^{reduced} reaction. Control reactions are devoid of any DMAP substrate. B) Rate of formation of spectral species 2 (see Fig 1f) in function of DMAP concentration. C) Rate of decay of spectral species 2 (see Fig 1f) in function of DMAP concentration. D) Spectral species obtained from singular value decomposition of rapid-scan stopped-flow spectrophotometric data following mixing of UbiX:prFMN^{reduced} with oxygenated buffer. E) The rate of purple radical (species B in panel d of this figure) formation as obtained from singular value decomposition of rapid-scan stopped-flow spectrophotometric data following mixing of UbiX:prFMN^{reduced} with oxygenated buffer has a linear dependence on oxygen concentration. Error bars are s.e.m. n=3

Europe PMC Funders Author Manuscripts

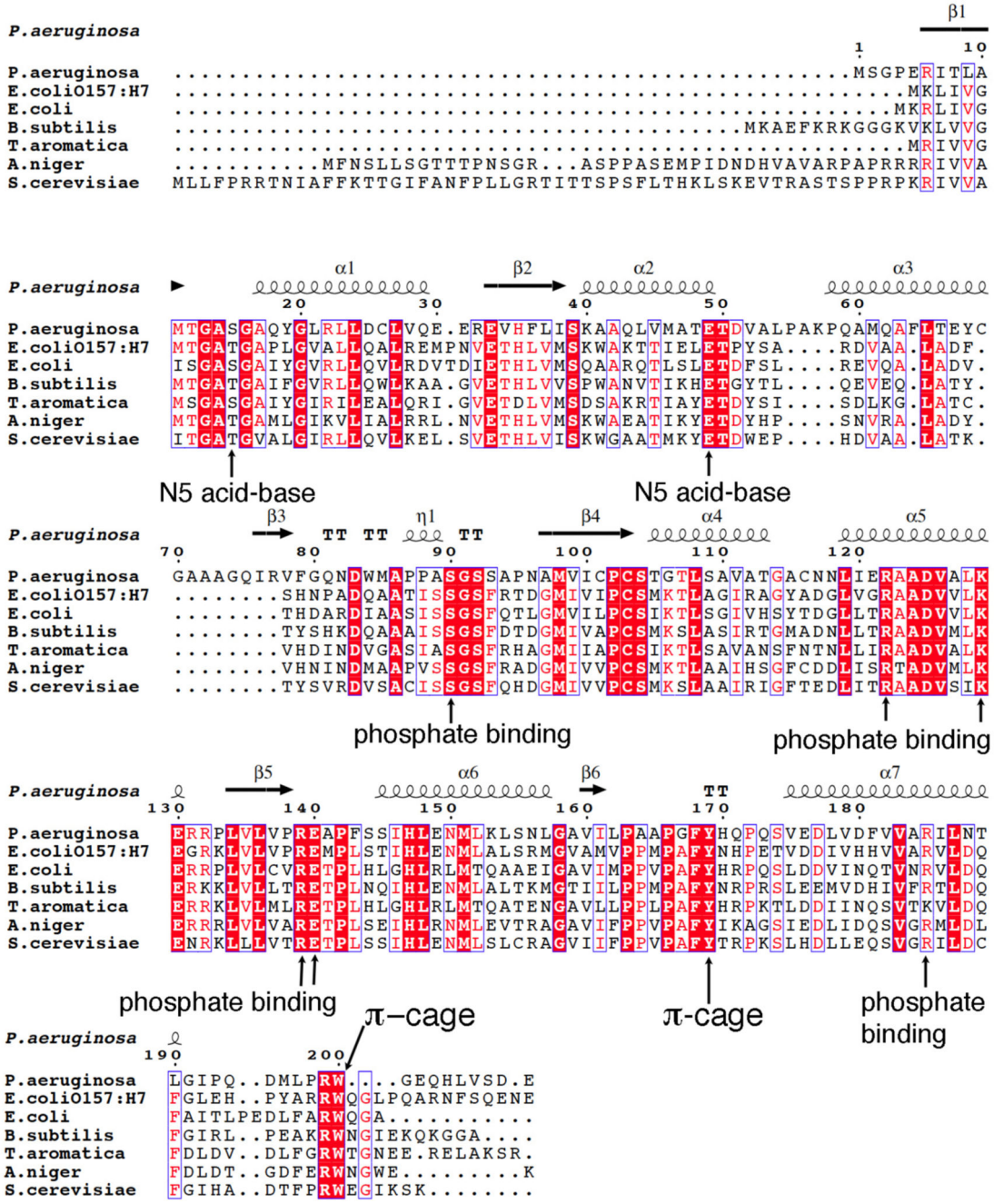

Extended Data Figure 6.

Multiple sequence alignment of UbiX/Pad enzymes from selected bacterial or fungal species. *Pseudomonas aeruginosa* UbiX (NP_252708), *Escherichia coli* O157:H7 EcdB (NP_311620), *Escherichia coli* UbiX (YP_490553), *Bacillus subtilis* BsdB (WP_009966530), *Saccharomyces cerevisiae* Pad1 (AAB64980), *Aspergillus niger* PadA1 (ABN13117), and orf8 from the *Thauera aromatica* phenylphosphate carboxylase gene cluster (PAAD_THAAR). Conserved residues involved in phosphate binding, N5 polar network or formation of the substrate binding p-cage are indicated by labelled arrows.

Secondary structure elements of *P. aeruginosa* UbiX crystal structure are shown. Alpha-helices and 3_{10}-helices (denoted as n) are shown as squiggles, β-strands by arrows and β-turns as TT.

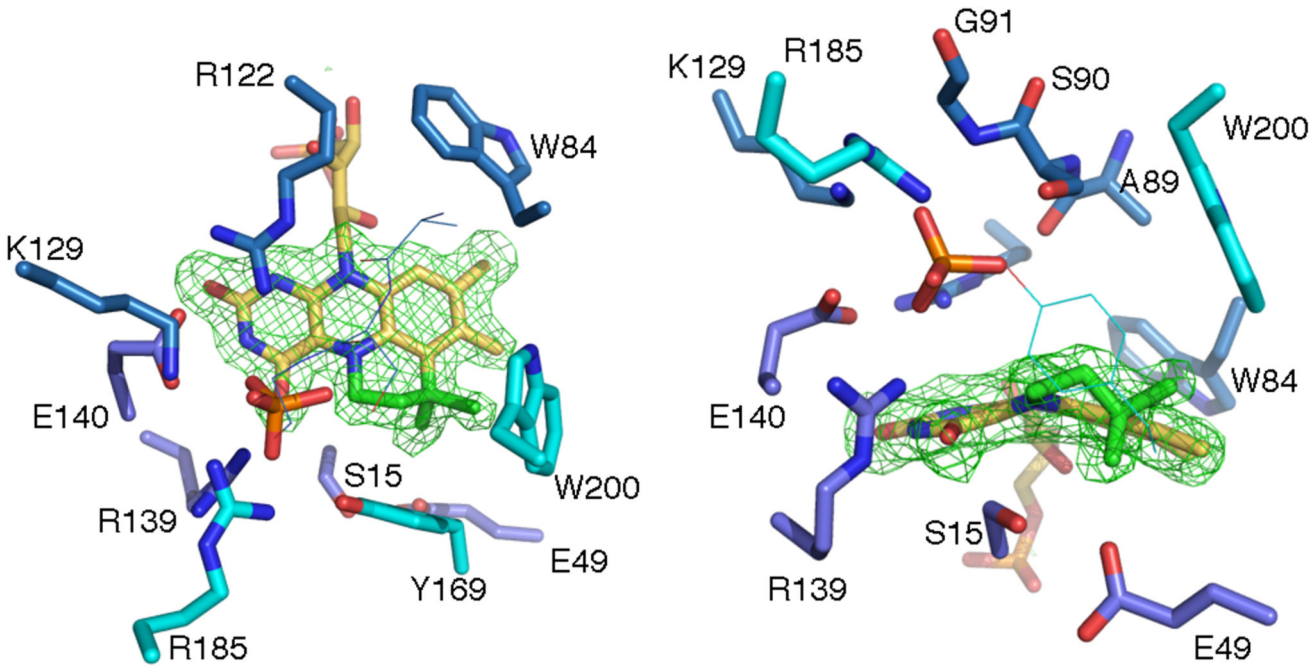

Extended Data Figure 7.

Crystal structure of *P. aeruginosa* UbiX:FMN:DMAP flash cooled to 100K at 30 s following complete reduction by sodium dithionite. Two orientations are displayed as in Fig 2. The omit map for the prFMN^{reduced} product is shown as green mesh, contoured at 4 sigma.

Europe PMC Funders Author Manuscripts

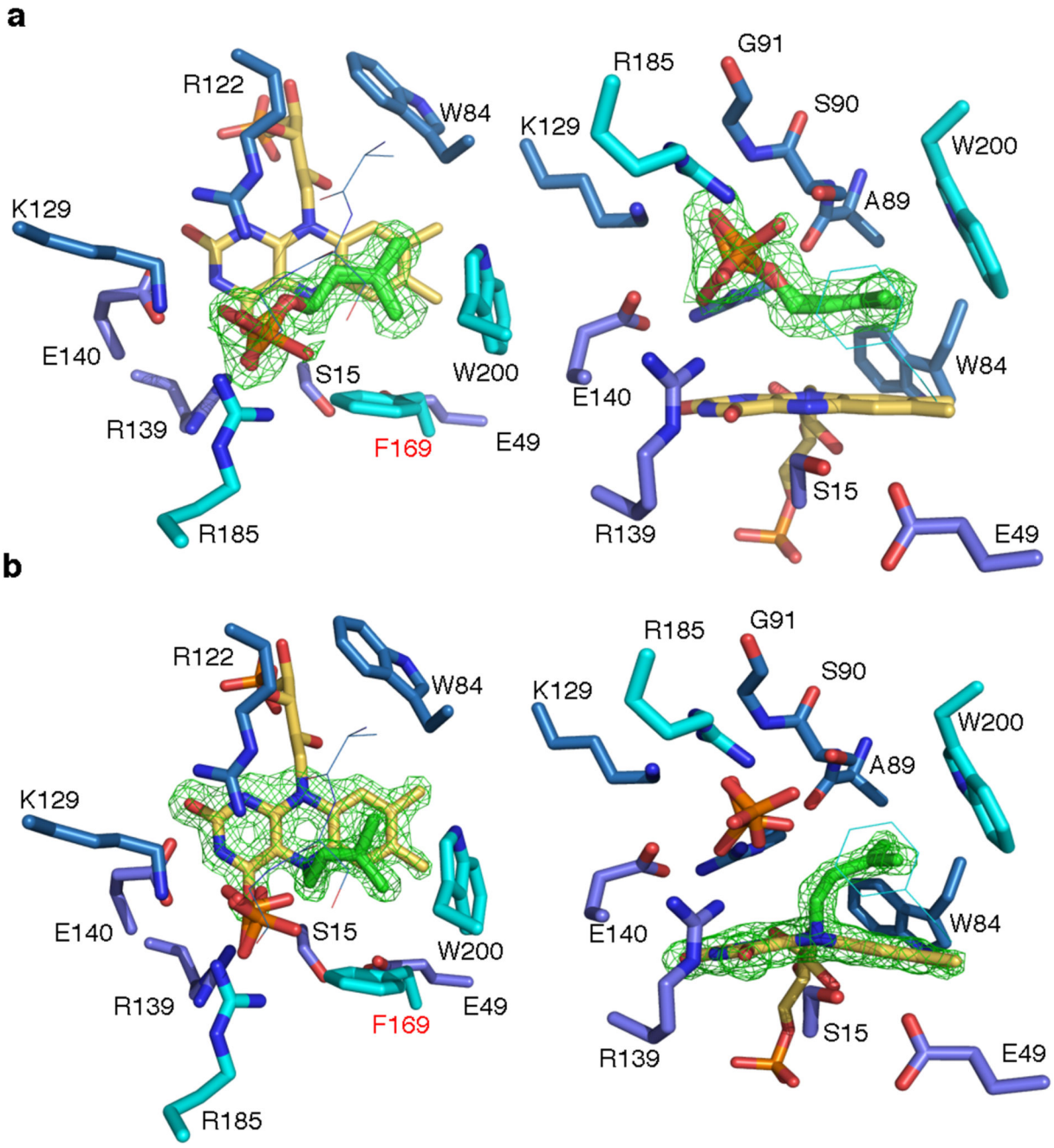

Extended Data Figure 8.

Crystal structures of *P. aeruginosa* UbiX^{Y169F} a) Detailed view of the UbiX^{Y169}:FMN:DMAP complex with individual amino acids contributing to active site structure shown in atom colored sticks (carbons colour coded as in Fig 2a). Two orientations are displayed as in Fig 2. The omit map for the DMAP substrate is shown as green mesh, contoured at 4 sigma. b) Detailed view of the UbiX^{Y169F} N5-C1' adduct species obtained through flash-cooling following reduction. The omit map for the N5-C1' adduct is shown as green mesh, contoured at 4 sigma.

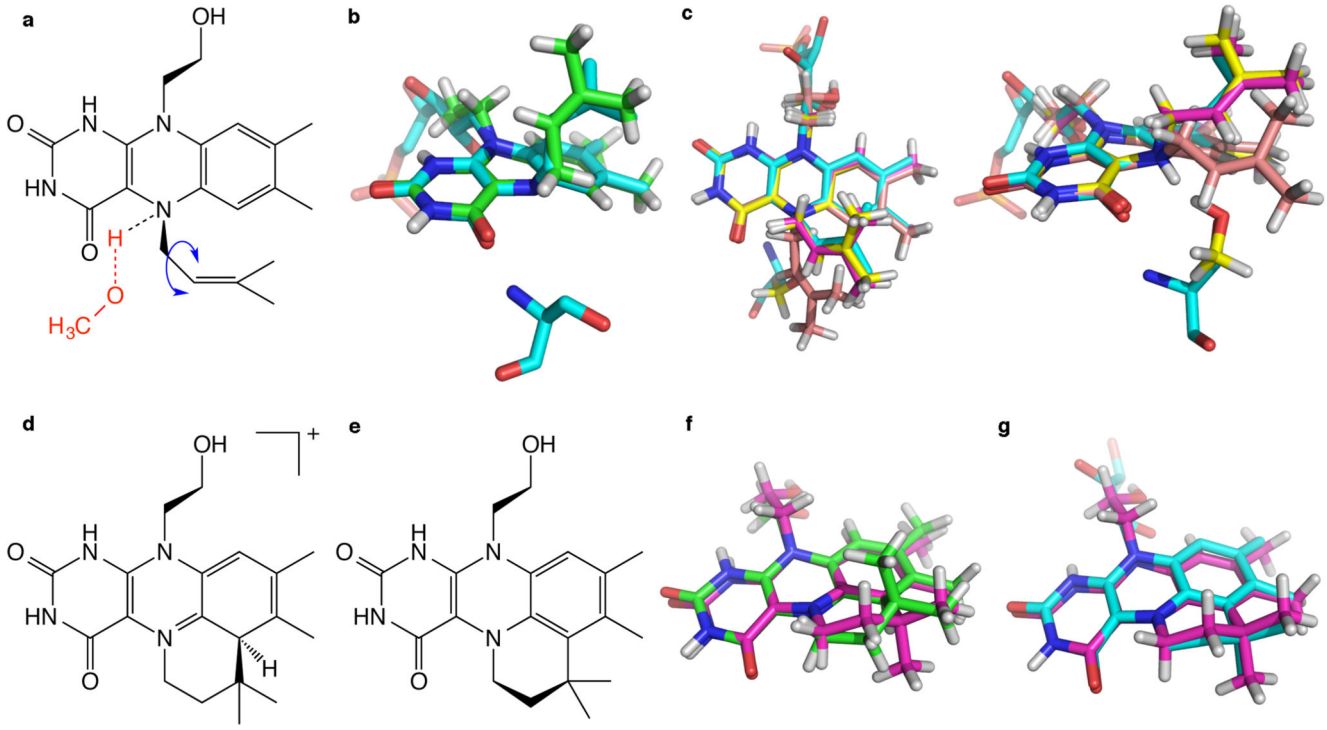

Extended Data Figure 9.

a) DFT models of species II and IVa (as defined in Fig 4). Conversion from II to IVa is achieved by ~180° rotation about C1'-C2' (blue arrow) and the N5-H and methanol species (red) are only found in species IVa models. b) Overlay of the species II DFT model (green carbons) with the crystal coordinates of species II and Ser15 (teal carbons). c) Three DFT models of IVa were examined and two orthogonal projections are shown overlaid with the crystal coordinates (teal carbons): (V*i*, yellow carbons) with a methanol analogue of Ser15 (a, in red) with the C-N5 distance fixed to the crystallographic distance of 4.0 Å; (V*ii*, magenta carbons) with N5 protonated (no methanol), and (V*iii*, light pink carbons) with N5 deprotonated and no methanol. DFT model of species V and VI are shown in d) and e), respectively and are overlaid in f) (V green carbons, VI magenta carbons). g). Overlay of the species VI DFT model (magenta carbons) with the crystal coordinates (teal carbons). Models were geometry optimised in the gas phase using the B3LYP/6-311++G(d,p) level of theory. Harmonic vibrational frequencies calculated using normal mode analysis were used to confirm that optimised geometries of all species were in local or global minima. In the case of species V*i*, 'ModRedundant' optimisation was performed to fix the C-N5 distance and one imaginary frequency of 67.60 cm^{-1} was observed. Cartesian coordinates of the optimised structures are given in Supplementary Information.

Europe PMC Funders Author Manuscripts

Extended Data Table 1

Data collection and refinement statistics

Ubix	**WT FMN:DMAP**	**WT N5 adduct 5 s following reduction**	**WT N5/C6 adduct, 30 s following reduction**	**WT N5/C6 adduct, co-crystallised (radical)**	**E49Q FMN:DMAP**	**E49Q $FMNH_2$:DMAP, < 5 s following reduction**	**E49Q N5 adduct > 15 s following reduction**	**Y169F FMN:DMAP**	**Y169F N5 adduct > 15 s following reduction**
PDB code	**4ZAF**	**4ZAV**	**4ZAW**	**4ZAX**	**4ZAG**	**4ZAL**	**4ZAY**	**4ZAN**	**4ZAZ**
Data collection									
Space group	F 2 3	F 2 3	F 2 3	F 2 3	F 2 3	F 2 3	F 2 3	F 2 3	F 2 3
Cell dimensions									
a, *b*, *c* (Å)	141.9	142.18	142.74	141.79	142.31	142.07	142.02	141.73	142.26
α, β, γ (°)	90	90	90	90	90	90	90	90	90
Resolution (Å)	70.92-1.71 (1.75-1.71)	50.27-1.40 (1.44-1.40)	43.04-1.89 (1.94-1.89)	42.75-1.61 (1.65-1.61)	32.65-1.68 (1.72-1.68)	42.84-1.62 (1.66-1.62)	32.58-1.54 (1.58-1.54)	70.86-1.76 (1.81-1.76)	50.30-1.45 (1.49-1.45)
R_{pim}	2.7 (29.8)	2.7 (29.7)	4.3 (33.0)	2.4 (33.5)	3.5 (35.6)	2.4 (29.2)	2.1 (26.6)	2.6 (36.0)	2.8 (35.6)
$I/\sigma I$	18.7 (2.8)	16 (2.7)	13.4 (2.7)	20.1 (2.5)	13.5 (2.2)	16.9 (2.8)	20.3 (3.0)	19.3 (2.4)	15.7 (2.4)
Completeness (%)	100 (100)	99.6 (100)	99.9 (99.9)	99.9 (100)	99.9 (99.9)	99.8 (100)	100 (100)	99.9 (100)	99.9 (99.9)
Redundancy	6.7 (6.8)	6.8 (6.8)	6.7 (6.7)	5.6 (5.4)	5.6 (5.5)	6.6 (6.7)	6.7 (6.7)	6.7 (6.4)	5.5 (5.4)
Refinement									
Resolution (Å)	70.95-1.71 (1.75-171)	50.27-1.40 (1.44-1.40)	43.04-1.89 (1.94-1.89)	42.75-1.61 (1.65-1.61)	32.65-1.68 (1.72-1.68)	42.84-1.62 (1.66-1.62)	32.58-1.54 (1.58-1.54)	70.86-1.76 (1.81-1.76)	50.30-1.45 (1.49-1.45)
No. refelections	24314 (1295)	44084 (2399)	18350 (990)	29027 (1541)	25816 (1402)	28593 (1525)	33304 (1756)	22355 (1074)	40068 (2066)
R_{work}/R_{free}	13.74/17.23	9.77/12.90	14.76/19.16	14.36/17.10	15.15/17.97	13.97/16.34	14.54/17.60	14.24/18.20	10.26/14.72
No. atoms									
Protein	1621	1627	1554	1620	1641	1664	1727	1593	1658
Ligand	41	36	36	36	41	41	36	41	36
Ion	13	18	13	14	4	6	15	7	20
Water	139	194	100	127	141	139	144	116	156
B-factors									
Protein	23.22	17.562	24.13	22.685	23.492	26.251	22.928	26.577	20.892
Ligand	20.21	14.938	19.286	26.107	21.486	23.631	19.212	21.411	17.141
Ion	38.34	29.653	30.154	25.756	25.435	60.387	28.885	34.894	28.034
Water	32.289	34.115	29.071	31.840	32.838	36.643	32.833	37.493	32.705
R.m.s deviations									
Bond length (Å)	0.0253	0.0258	0.0209	0.0260	0.0229	0.0262	0.0262	0.0222	0.0250
Bond angles (°)	2.1189	1.9826	1.9719	2.4312	2.1375	2.3693	2.3773	2.4068	2.2280

Supplementary Material

Refer to Web version on PubMed Central for supplementary material.

Acknowledgements

This work was supported by BBSRC grants (BB/K017802/1 with Shell and BB/M017702/1). We thank Diamond Light Source for access to beamlines (proposal number MX8997) that contributed to the results presented here. S.H. is a BBSRC David Phillips research fellow. NSS is an EPSRC Established Career Fellow and Royal Society Wolfson Award holder. The authors acknowledge the assistance given by IT Services and the use of the Computational Shared Facility and the Protein Structure Facility at The University of Manchester.

References

1. Lenaz G, Genova ML. Mobility and function of coenzyme Q (ubiquinone) in the mitochondiral respiratory chain. Biochim Biophys Acta. 2009; 1787:563–573. [PubMed: 19268424]
2. Aussel L, Pierrel F, Loiseau L, Lombard M, Fontecave M, Barras F. Biosynthesis and physiology of coenzyme Q in bacteria. Biochim Biophys Acta. 2014; 1837:1004–1011. [PubMed: 24480387]
3. Gulmezian M, Hyman KR, Marbois BN, Clarke CF, Javor GT. The role of UbiX in *Escherichia coli* coenzyme Q biosynthesis. Arch Biochem Biophys. 2007; 467:144–153. [PubMed: 17889824]
4. Rangarajan ES, Li Y, Iannuzzi P, Tocilj A, Hung LW, Matte A, Cygler M. Crystal structure of a dodecameric FMN-dependent UbiX-like decarboxylate (Pad1) from *Eschericia coli* O157:H7. Protein Sci. 2004; 13:3006–3016. [PubMed: 15459342]
5. Payne KAP, et al. A new cofactor supports reversible decarboxylation of α, β-unsaturated acids reminiscent of 1,3-dipolar cycloaddition chemistry. Nature. in press.
6. Liang PH. Reaction kinetics, catalytic mechanisms, conformational changes, and inhibitor design for prenyltransferases. Biochemistry. 2009; 48:6562–6570. [PubMed: 19537817]
7. Doud EH, Perlstein DL, Wolpert M, Cane DE, Walker S. Two distinct mechanisms for TIM barrel prenyltransferases in bacteria. J Am Chem Soc. 2011; 133:1270–1273. [PubMed: 21214173]
8. Gao Y, Honzatko RB, Peters. Terpenoid synthase structures: a so far complete view of complex catalysis. Nat Prod Rep. 2012; 29:1153–1175. [PubMed: 22907771]
9. Walsh CT, Wencewicz TA. Flavoenzymes: versatile catalysts in biosynthetic pathways. Nat Prod Rep. 2013; 30:175–200. [PubMed: 23051833]
10. Heuts DP, Scrutton NS, McIntire WS, Fraaije MW. What's in a covalent bond? On the role and formation of covalently bound flavin cofactors. FEBS J. 2009; 276:3405–3427. [PubMed: 19438712]
11. Mukai N, Masaki K, Fujii T, Kawamukai M, Iefuji H. PAD1 and FDC1 are essential for the decarboxylation of phenylacrylic acids in *Saccharomyces cerevisiae*. J Biosci Bioeng. 2010; 109:564–569. [PubMed: 20471595]
12. Lin F, Ferguson KL, Boyer DR, Lin XN, Marsh EN. Isofunctional enzymes Pad1 and UbiX catalyse formation of a novel cofactor required by ferulic acid decarboxylase and 4-hydroxy-3-polyprenylbenzoic acid decarboxylase. ACS Chem Biol. 2015 In press.
13. Kopec J, Schnell R, Schneider G. Structure of PA4019, a putative aromatic acid decarboxylase from *Pseudomonas aeruginosa*. Acta Crystallogr Sect F. 2011; 67:1184–1188.
14. Fraaije MW, Mattevi A. Flavoenzymes: diverse catalysts with recurrent features. Trends Biochem Sci. 2000; 25:126–132. [PubMed: 10694883]
15. Berthelot K, Estevez Y, Deffieux A, Peruch F. Isopentenyl diphosphate isomerase: A checkpoint to isoprenoid biosynthesis. Biochimie. 2012; 94:1621–1634. [PubMed: 22503704]
16. Nagai T, Unno H, Janczak MW, Yoshimura T, Poulter CD, Hemmi H. Covalent modification of reduced flavin mononucleotide in type-2 isopentenyl diphosphate isomerase by active-site-directed inhibitors. Proc Natl Acad Sci USA. 2011; 108:20461–20466. [PubMed: 22158896]
17. Christianson DW. Unearthing the roots of the terpenome. Curr Opin Chem Biol. 2008; 12:141–150. [PubMed: 18249199]

18. Smanski MJ, Peterson RM, Huang SX, Shen B. Bacterial diterpene synthases: new opportunities for mechanistic enzymology and engineered biosynthesis. Curr Opin Chem Biol. 2012; 16:132–141. [PubMed: 22445175]
19. Lupa B, Lyon D, Gibbs MD, Reeves RA, Wiegel J. Distribution of genes encoding the microbial non-oxidative reversible hydroxyarylic acid decarboxylates/phenol carboxylases. Genomics. 2005; 86:342–351. [PubMed: 15979273]
20. Abu Laban N, Selesi D, Rattie T, Tischler P, Meckenstock RU. Identification of enzymes involved in anaerobic benzene degradation by a strictly anaerobic iron-reducing enrichment culture. Environ Microbiol. 2010; 12:2783–2796. [PubMed: 20545743]
21. Erb TJ. Carboxylases in natural and synthetic microbial pathways. Appl Environ Microbiol. 2011; 77:8466–8477. [PubMed: 22003013]
22. Chang WC, Song H, Liu HW, Liu P. Current development in isoprenoid precursor biosynthesis and regulation. Curr Opin Chem Biol. 2013; 17:571–579. [PubMed: 23891475]
23. Vannice JC, Skaff DA, Keightley A, Addo JK, Wyckoff GJ, Miriorko HM. Identification in *Haloferax volcanii* of phosphomevalonate decarboxylase and isopentenyl phosphate kinase as catalysts of the terminal enzyme reactions in an archaeal alternate mevalonate pathway. J Bacteriol. 2014; 196:1055–1063. [PubMed: 24375100]
24. Sobrado P. Noncanonical reactions of flavoenzymes. Int J Mol Sci. 2012; 13:14219–14242. [PubMed: 23203060]
25. Sun HG, Ruszczycky MW, Chang WC, Thibodeaux CJ, Liu HW. Nucleophilic participation of reduced flavin coenzyme in mechanism of UDP-galactopyranose mutase. J Biol Chem. 2012; 287:4602–4608. [PubMed: 22187430]
26. Winn MD, et al. Overview of the CCP4 suite and current developments. Acta Crystallogr. 2011; D67:235–242.
27. Kabsch W. XDS. Acta Crystallogr. 2010; D66:125–132.
28. Fu G, et al. Atomic-Resolution Structure of an N(5) Flavin Adduct in D-Arginine Dehydrogenase. Biochemistry. 2011; 50:6292–6294. [PubMed: 21707047]
29. Frisch MJ, et al. Gaussian 09 (Gaussian, Wallingford, CT revision B.01). 2010
30. Guex N, Peitsch MC. SWISS-MODEL and the Swiss-PdbViewer: An environment for comparative protein modeling. Electrophoresis. 1997; 18:2714–2723.http://www.expasy.org/spdbv/ [PubMed: 9504803]

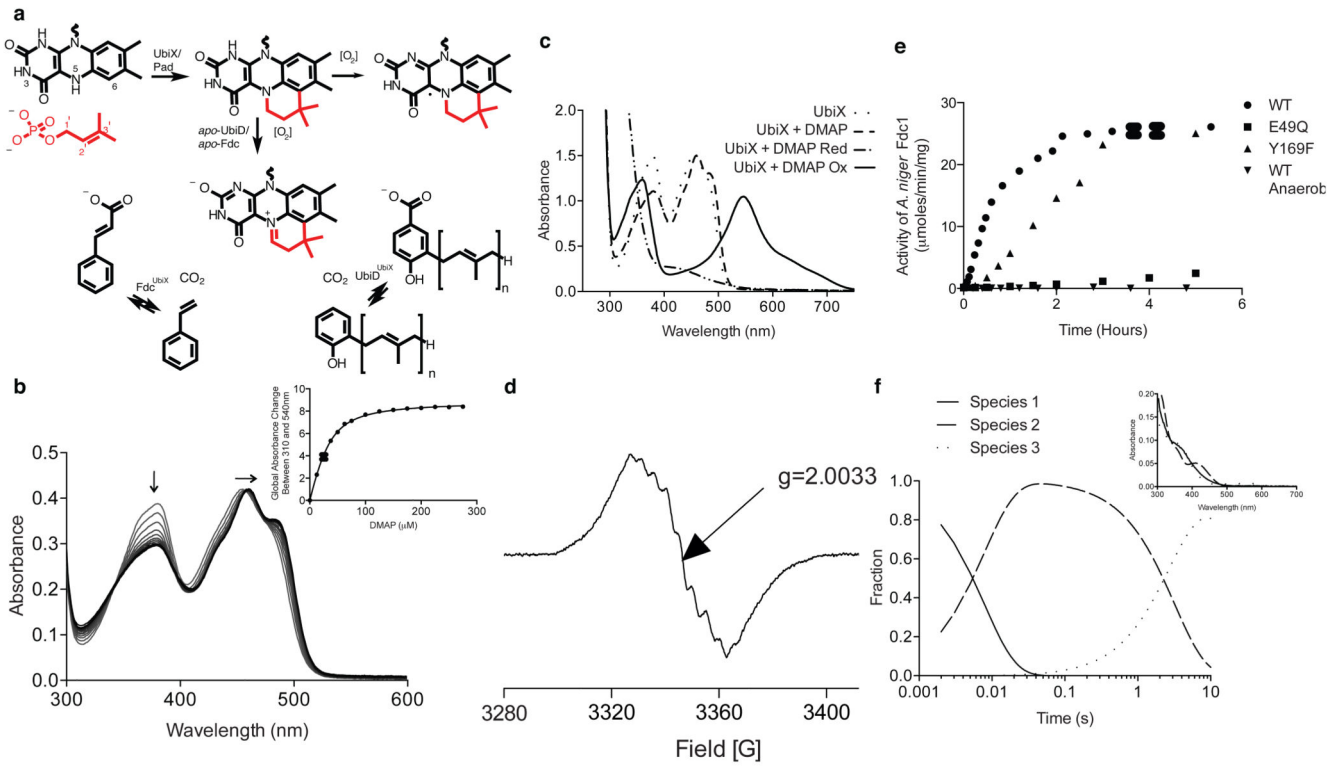

Fig 1.

P. aeruginosa UbiX solutions studies. **a**) Schematic overview of the proposed UbiX reaction. The N5-C6 prenylated $FMNH_2$ product ($prFMN^{reduced}$) undergoes (likely non-physiological) oxidation to a radical species ($prFMN^{radical}$) in presence of oxygen (see panel **d**). In presence of apo-UbiD or apo-Fdc1, we propose the UbiX product is oxidized to the UbiD/Fdc1 $prFMN^{iminium}$ cofactor (see panel **e**). **b**) Titration of oxidized FMN-UbiX with dimethylallylmonophosphate. Grey lines represent individual scans at increasing [DMAP] concentrations with the black line representing the final spectrum obtained at saturation. An binding curve is derived from the global absorbance change in the 310-450nm range. **c**) UV-visible spectra of UbiX:FMN obtained during redox cycling in presence of DMAP **d**) EPR spectrum of the UbiX:$prFMN^{radical}$ complex **e**) Reconstitution of *A. niger apo*-Fdc1 decarboxylase activity by incubation with WT and variant UbiX enzymes in presence of DMAP and $FMNH_2$ followed by oxygen exposure. No activity can be observed under anaerobic conditions. **f**) Singular value decomposition of rapid-scan stopped-flow spectrophotometric data following mixing of WT UbiX:$FMNH_2$ with DMAP. The spectral species identified can tentatively be assigned to 1: ternary UbiX:$FMNH_2$:DMAP complex, 2: an intermediate covalent adduct formed between $FMNH_2$ and DMAP and 3: the UbiX:$prFMN^{reduced}$ product.

Europe PMC Funders Author Manuscripts

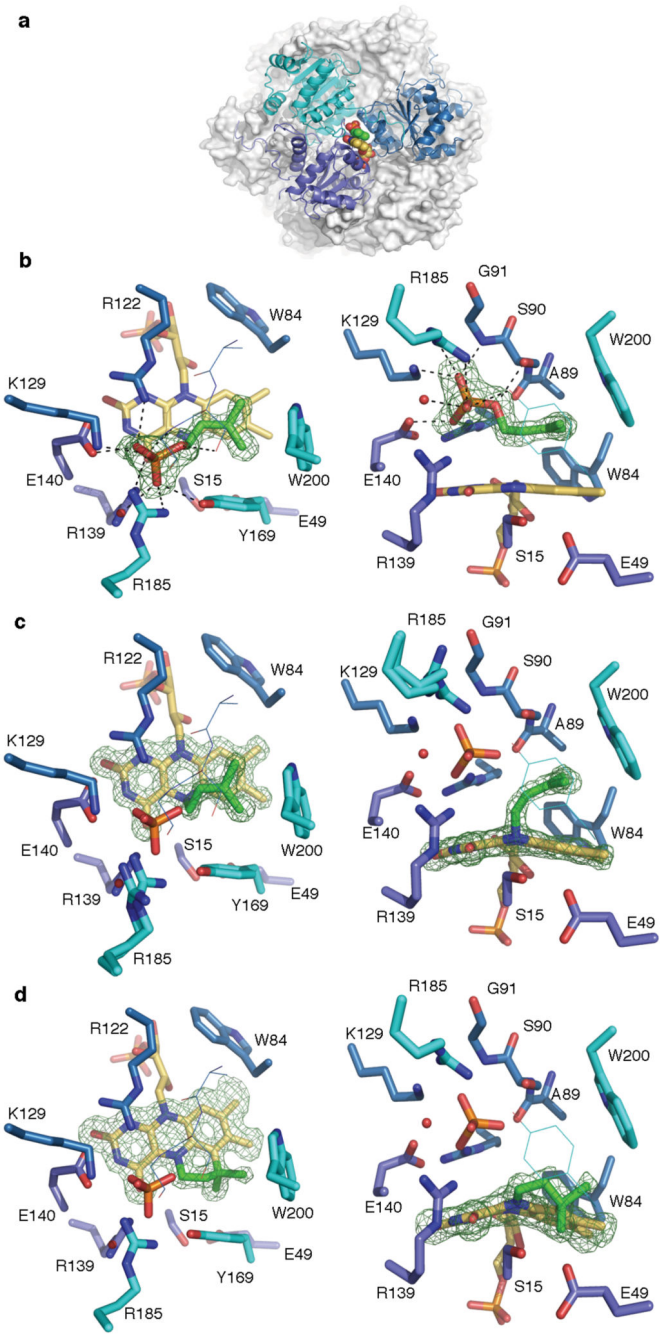

Fig 2.

Crystal structures of *P. aeruginosa* UbiX. **a**) Overview of the dodecameric UbiX structure, with 3 individual monomers (colored in cyan, blue and teal respectively) contributing to a single active site shown in cartoon representation while the remainder (in grey) is shown in surface representation. The bound FMN and DMAP substrates are shown in atom colored spheres. **b**) Detailed view of the oxidised UbiX:FMN:DMAP complex in two orientations related by 90 degree rotation along the horizontal axis. Individual amino acids contributing to active site structure shown in atom colored sticks (carbons colour coded as in Fig 2a).

Residues positioned in front of the FMN:DMAP substrates are shown as thin lines for clarity. The omit map for the DMAP substrate is shown as green mesh, contoured at 4 sigma. Hydrogen bonding networks established with the phosphate moiety are shown by dotted lines. **c**) Detailed view of the N5-C1' alkyl adduct species (in two orientations related by a 90 degree rotation along the horizontal axis) obtained through rapid flash-cooling following reduction. The omit map for the N5-C1' adduct is shown as a green mesh, contoured at 4 sigma. **d**) Detailed view of the UbiX:product complex in two orientations related by a 90 degree rotation along the horizontal axis. The omit map for the product is shown as green mesh, contoured at 3.5 sigma.

Europe PMC Funders Author Manuscripts

Europe PMC Funders Author Manuscripts

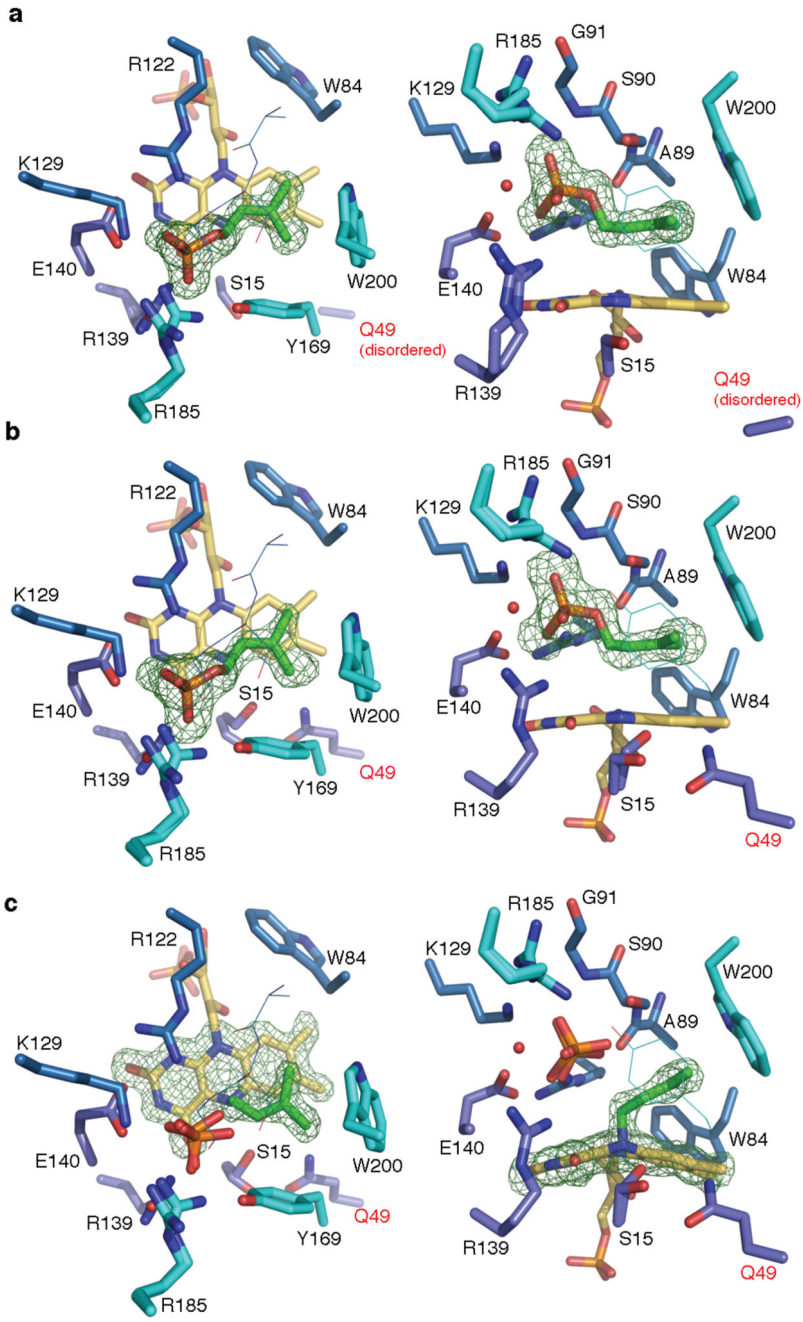

Fig 3.

Crystal structures of *P. aeruginosa* UbiX^{E49Q} **a**) Detailed view of the UbiX^{E49Q}:FMN:DMAP complex with individual amino acids contributing to active site structure shown in atom colored sticks (carbons colour coded as in Fig 2a). Two orientations are displayed as in Fig 2. The omit map for the DMAP substrate is shown as green mesh, contoured at 4 sigma. **b**) Detailed view of the UbiX^{E49Q}:FMNH$_2$:DMAP complex obtained through rapid flash-cooling following reduction. The omit map for the DMAP substrate is shown as green mesh, contoured at 3 sigma. **c**) Detailed view of the UbiX^{E49Q} N5-C1' alkyl

adduct species obtained through flash-cooling following reduction. The omit map for the N5-C1’ adduct is shown as green mesh, contoured at 4 sigma.

Europe PMC Funders Author Manuscripts

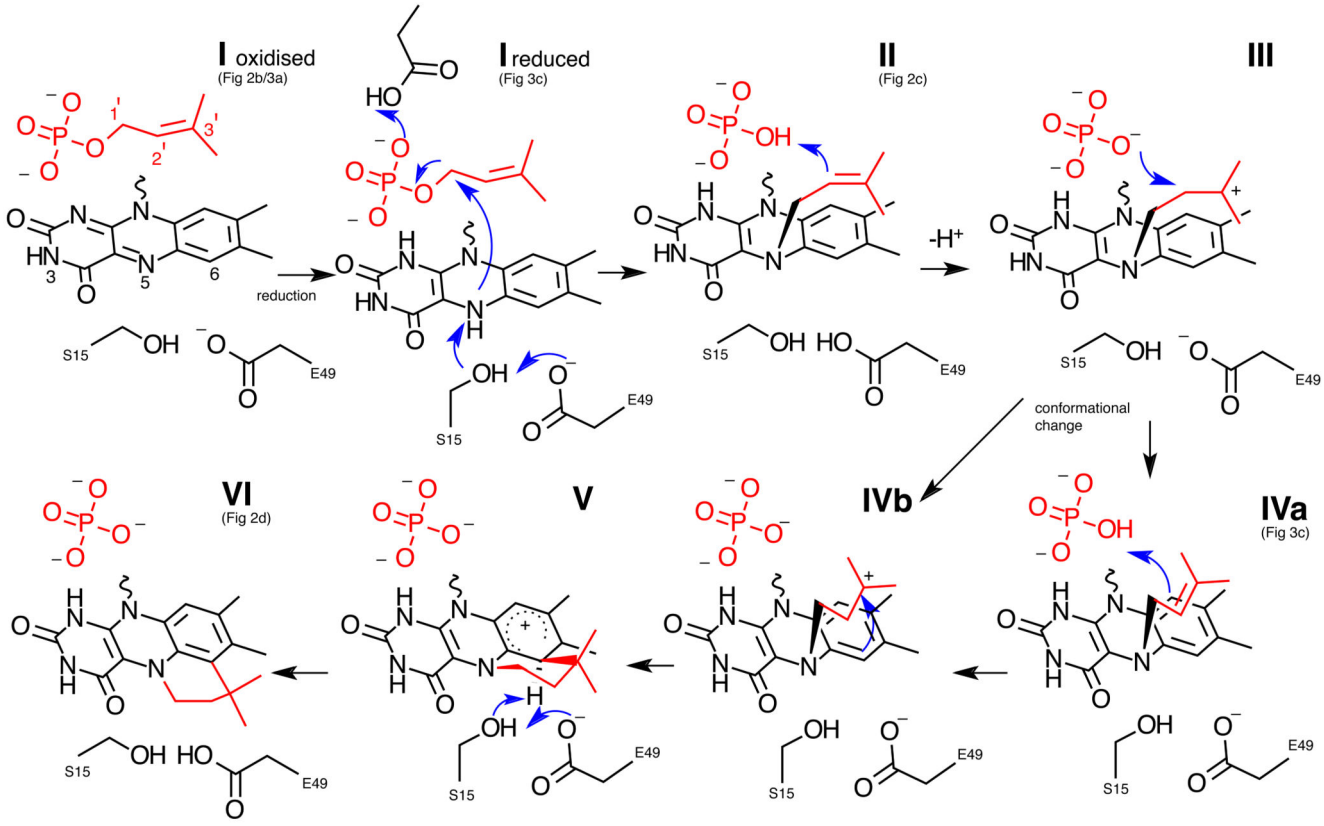

Fig 4.

Schematic representation of the proposed UbiX mechanism. DMAP derived atoms are shown in red. Roman numerals indicate the various intermediate species proposed (see main text). References to individual figures below roman numerals refer to corresponding crystal structures are obtained for the WT or UbiX^{E49Q} mutant.

Europe PMC Funders Author Manuscripts

Europe PMC Funders Author Manuscripts

Extended Data Table 1

Data collection and refinement statistics

Ubix	**WT FMN:DMAP**	**WT N5 adduct 5 s following reduction**	**WT N5/C6 adduct, 30 s following reduction**	**WT N5/C6 adduct, co-crystallised (radical)**	**E49Q FMN:DMAP**	**E49Q $FMNH_2$:DMAP, < 5 s following reduction**	**E49Q N5 adduct > 15 s following reduction**	**Y169F FMN:DMAP**	**Y169F N5 adduct > 15 s following reduction**
PDB code	**4ZAF**	**4ZAV**	**4ZAW**	**4ZAX**	**4ZAG**	**4ZAL**	**4ZAY**	**4ZAN**	**4ZAZ**
Data collection									
Space group	F 2 3	F 2 3	F 2 3	F 2 3	F 2 3	F 2 3	F 2 3	F 2 3	F 2 3
Cell dimensions									
a, *b*, *c* (Å)	141.9	142.18	142.74	141.79	142.31	142.07	142.02	141.73	142.26
α, β, γ (°)	90	90	90	90	90	90	90	90	90
Resolution (Å)	70.92-1.71 (1.75-1.71)	50.27-1.40 (1.44-1.40)	43.04-1.89 (1.94-1.89)	42.75-1.61 (1.65-1.61)	32.65-1.68 (1.72-1.68)	42.84-1.62 (1.66-1.62)	32.58-1.54 (1.58-1.54)	70.86-1.76 (1.81-1.76)	50.30-1.45 (1.49-1.45)
R_{pim}	2.7 (29.8)	2.7 (29.7)	4.3 (33.0)	2.4 (33.5)	3.5 (35.6)	2.4 (29.2)	2.1 (26.6)	2.6 (36.0)	2.8 (35.6)
$I/\sigma I$	18.7 (2.8)	16 (2.7)	13.4 (2.7)	20.1 (2.5)	13.5 (2.2)	16.9 (2.8)	20.3 (3.0)	19.3 (2.4)	15.7 (2.4)
Completeness (%)	100 (100)	99.6 (100)	99.9 (99.9)	99.9 (100)	99.9 (99.9)	99.8 (100)	100 (100)	99.9 (100)	99.9 (99.9)
Redundancy	6.7 (6.8)	6.8 (6.8)	6.7 (6.7)	5.6 (5.4)	5.6 (5.5)	6.6 (6.7)	6.7 (6.7)	6.7 (6.4)	5.5 (5.4)
Refinement									
Resolution (Å)	70.95-1.71 (1.75-171)	50.27-1.40 (1.44-1.40)	43.04-1.89 (1.94-1.89)	42.75-1.61 (1.65-1.61)	32.65-1.68 (1.72-1.68)	42.84-1.62 (1.66-1.62)	32.58-1.54 (1.58-1.54)	70.86-1.76 (1.81-1.76)	50.30-1.45 (1.49-1.45)
No. refelections	24314 (1295)	44084 (2399)	18350 (990)	29027 (1541)	25816 (1402)	28593 (1525)	33304 (1756)	22355 (1074)	40068 (2066)
R_{work}/R_{free}	13.74/17.23	9.77/12.90	14.76/19.16	14.36/17.10	15.15/17.97	13.97/16.34	14.54/17.60	14.24/18.20	10.26/14.72
No. atoms									
Protein	1621	1627	1554	1620	1641	1664	1727	1593	1658
Ligand	41	36	36	36	41	41	36	41	36
Ion	13	18	13	14	4	6	15	7	20
Water	139	194	100	127	141	139	144	116	156
B-factors									
Protein	23.22	17.562	24.13	22.685	23.492	26.251	22.928	26.577	20.892
Ligand	20.21	14.938	19.286	26.107	21.486	23.631	19.212	21.411	17.141
Ion	38.34	29.653	30.154	25.756	25.435	60.387	28.885	34.894	28.034
Water	32.289	34.115	29.071	31.840	32.838	36.643	32.833	37.493	32.705
R.m.s deviations									
Bond length (Å)	0.0253	0.0258	0.0209	0.0260	0.0229	0.0262	0.0262	0.0222	0.0250
Bond angles (°)	2.1189	1.9826	1.9719	2.4312	2.1375	2.3693	2.3773	2.4068	2.2280